Supplementary Material for "Superconductivity beyond the conventional Pauli limit in high-pressure $CeSb_2$"

IN-PLANE UPPER CRITICAL FIELD

All the high pressure critical field data presented in the main manuscript were taken with the magnetic field applied along the crystallographic c-direction, as defined for the low pressure structure of $CeSb_2$. To check for anisotropy of the upper critical field B_{c2} for different field directions, $B_{c2}(T)$ has also been determined with the pressure cell mounted sideways in the cryostat, so that the field is applied perpendicular to the c-direction, or within the $a-b$ plane. The effect of a magnetic field applied in the $a-b$ plane on the superconducting transition at 34.2 kbar is shown in Fig. 1. The lower panel in Fig. 1 illustrates that the initial slope $B'_{c2} \simeq 30\,\mathrm{T\,K^{-1}}$, similar to the initial slope determined for field along c at the close-by pressure of 34.9 kbar. Moreover, the in-plane upper critical field exceeds the Pauli limit $B_{\mathrm{Pauli}} = 0.42\,\mathrm{T}$, but it is slightly smaller than the c-axis critical field, reaching about 1.5 T at about 0.13 K compared to the c-axis critical field, which at 34.9 kbar exceeds 1.5 T at about 0.16 K (Fig. 3f in main paper). At least at this pressure, for $p > p_c$, the anisotropy in the response to applied field appears to be minor, but further studies over a wider range of pressures and exploring the anisotropy for more field directions are now under way.

CRYSTALLINITY ACROSS THE STRUCTURAL TRANSITION

No high pressure single crystal x-ray diffraction data is at present available. To determine whether the pressure-induced structural transition preserves the crystallinity of the starting single crystals of $CeSb_2$, we can, however, turn to resistance measurements under different magnetic field directions (Fig. 2). Measurements at a pressure of 24.6 kbar, well above the pressure at which the structural transition is complete, display a pronounced anisotropy in the resistivity under applied field. The differences between the two resistivity traces recorded with the field along the c direction (as defined for the $p = 0$ structure) and with the field perpendicular to the c direction strongly suggest that $CeSb_2$ samples retain their crystallinity on crossing the structural transition. The slight anisotropy in the superconducting upper critical field discussed in the preceding section further supports this interpretation.

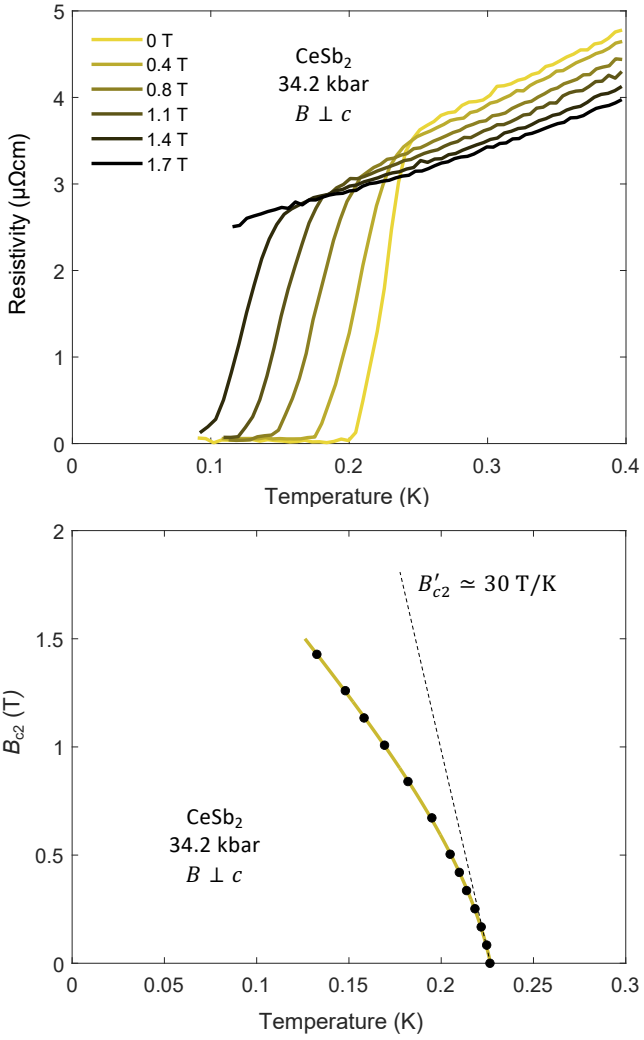

Figure 1. The effect of an in-plane applied magnetic field on the superconducting transition of $CeSb_2$ at 34.2 kbar. (Top) resistive transitions recorded at different values of the in-plane applied magnetic field. (Bottom) The resulting temperature dependence of the upper critical field B_{c2} determined from the mid-points of the resistive transitions. The initial slope of order $30\,\mathrm{T\,K^{-1}}$ is similar to the value determined for $c-$axis fields at the nearby pressure of 34.9 kbar

ESTIMATES BASED ON THE ORBITAL LIMITING FIELD

In $CeSb_2$, the analysis of the upper critical field for $p < 33$ kbar is complicated by the unusual inverted S-shape of the critical field curve, but at higher pressures the critical field follows a more conventional temperature dependence.

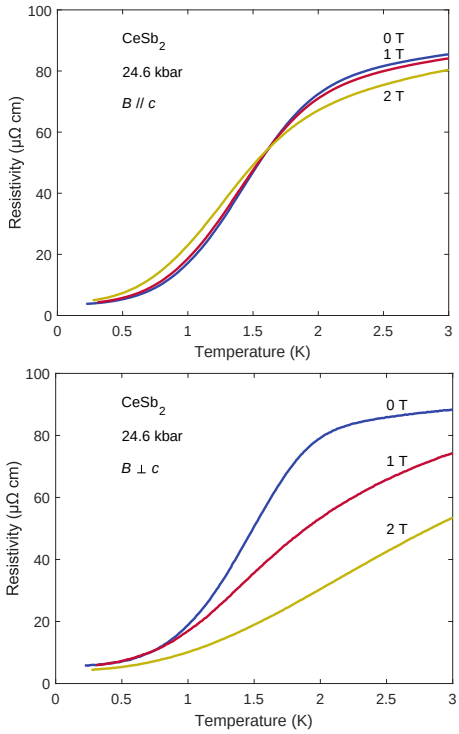

Figure 2. Low temperature resistivity versus temperature under applied field recorded at a pressure well above the pressure at which the structural transition is complete, in two samples mounted (a) such that the applied field is along the c-direction, and (b) with the field perpendicular to the c-direction. The pronounced differences between the two sets of curves suggest that $CeSb_2$ samples do not become polycrystalline on crossing the pressure-induced structural transition.

Estimates for coherence length, Fermi velocity and effective mass

At 34.9 kbar, we extract an initial slope $B'_{c2} \simeq 30\,\mathrm{T\,K^{-1}}$, which together with $T_c \simeq 0.22\,\mathrm{K}$ allows an estimate for the orbitally limited upper critical field $B_{c2}^{(o)} = 0.73 B'_{c2} T_c \simeq 5\,\mathrm{T}$ [1].

Following standard theory (e.g. [2]), this orbitally-limited critical field corresponds to a superconducting coherence length

$$\xi_0 = \sqrt{\Phi_0 / \left(2\pi B_{c2}^{(o)}\right)} \simeq 82\,\text{Å}\ , \tag{1}$$

where $\Phi_0 = h/(2e)$ is the quantum of flux. We compare this to the BCS coherence length, which we obtain from

$$\xi_{\mathbf{BCS}} = \frac{\hbar v_F}{\pi \Delta} \tag{2}$$

[2, 3], where v_F is the Fermi velocity and Δ is the superconducting gap. The relation linking gap and transition temperature, $\Delta = \eta k_B T_c$ with $\eta = 1.76$ in BCS theory, then leads to an estimate for the Fermi velocity in high pressure $CeSb_2$ of $v_F \simeq 1300\,\mathrm{m\,s^{-1}}$.

The Fermi surface geometry in high pressure $CeSb_2$ is not yet known, but the lattice density of about 1 formula unit/80 Å^3 suggests $k_F \simeq 0.7\,\text{Å}^{-1}$, a typical value for a metal. The Fermi momentum $\hbar k_F = m^* v_F$ then indicates an effective mass $m^* \simeq 610 m_e$, where m_e is the bare electron mass.

Relation to effective mass and Sommerfeld coefficient

By combining Equation 1 and Equation 2 above, we can obtain an expression for the ratio $\sqrt{B'_{c2}/T_c}$:

$$\begin{aligned}\xi &= \sqrt{\frac{\Phi_0}{2\pi B_{c2}^{(o)}}} = \sqrt{\frac{\Phi_0}{2\pi 0.73 B'_{c2} T_c}} \\ &= \frac{\hbar v_F}{\pi\Delta} = \frac{\hbar v_F}{\pi \eta k_B T_c} \implies \\ \sqrt{\frac{B'_{c2}}{T_c}} &= \sqrt{\frac{\pi\Phi_0}{1.46}}\,\frac{\eta k_\mathrm{B}}{\hbar v_F}\,.\end{aligned} \tag{3}$$

Setting $m^* v_F = \hbar k_F$ then enables comparison to other materials:

$$\sqrt{\frac{B'_{c2}}{T_c}} = \sqrt{\frac{\pi\Phi_0}{1.46}}\,\frac{\eta k_\mathrm{B}}{\hbar^2}\,\frac{m^*}{k_F}\,. \tag{4}$$

This shows that the ratio $\sqrt{B'_{c2}/T_c}$ depends only on the effective mass and on the Fermi wavevector k_F. Because k_F in turn depends primarily on the lattice density and varies much less between good metals than m^*, $\sqrt{B'_{c2}/T_c}$ provides a handle for comparing the mass enhancements in different materials. Moreover, m^* and k_F also relate to the electronic density of states and thereby to the Sommerfeld ratio of the heat capacity. If we approximate the Fermi surface by p spheres of equal radius k_F with isotropic effective mass m^*, the standard result for the heat capacity Sommerfeld ratio $C/T = \frac{\pi^2}{3} k_B^2 g(E_F)$, where $g(E_F)$ is the density of states per mol at the Fermi level, translates to

$$C/T = p\frac{\pi^2 m^*}{\hbar^2 k_F^2} k_B R\,, \tag{5}$$

with R the molar gas constant. This can be combined with Equation 4 into a ratio independent of the effective mass m^* or Fermi velocity v_F:

$$\frac{C/T}{\sqrt{B'_{c2}/T_c}} = p\frac{\pi^{3/2}}{\eta k_F}\sqrt{\frac{1.46}{\Phi_0}}R\,. \tag{6}$$

This ratio is approximately $0.1\,\mathrm{J/(molKT^{1/2})}$ for $p = 1$ and $\eta = 1.76$. The critical field and Sommerfeld ratio

data in Table 1 of the main paper are roughly consistent with this analysis. Extending it also to $CeSb_2$ leads to an estimate for the Sommerfeld coefficient at 34.9 kbar of $C/T \simeq 1.2\,\mathrm{J/(molK^2)}$.

Mean free path

The mean free path in our samples can be estimated (e.g. [3]) from the Drude theory result $\ell = 6\pi^2\hbar/\left(e^2\rho_0 S_F\right) = 15,300\text{Å}\,(\rho_0/\mu\Omega\text{cm})^{-1}\left(S_F/\text{Å}^{-2}\right)^{-1}$, where S_F now includes the total Fermi surface area, which in the spirit of the previous section we estimate as $S_F = p4\pi k_F^2 \simeq 6\ \text{Å}^{-2}$. For samples with residual resistivity $\rho_0 \simeq 5\,\mu\Omega\,\text{cm}$, this gives a mean free path of $\ell \simeq 510\,\text{Å}$. As the mean free path far exceeds the coherence length $\xi_0 \simeq 82\,\text{Å}$ estimated above from the critical field data, high pressure $CeSb_2$ can be assumed to be in the clean limit.

THE SIGN REVERSAL IN dB_{c2}/dT

Applying the Clausius-Clapeyron argument to $B_{c2}(T)$ yields for a second-order transition $dB_{c2}/dT = -(C_s - C_n)/T(\partial M_s/\partial T - \partial M_n/\partial T)$, with C the specific heat capacity, M the magnetization and the subscripts s and n denoting superconducting and normal states, respectively. Around the second-order transition, the heat capacity of the superconducting state C_s must be higher than that of the normal state. Therefore, the observed $dB_{c2}/dT > 0$ requires $\partial M_s/\partial T < \partial M_n/\partial T$ or, applying a Maxwell relation, $\partial S_s/\partial B < \partial S_n/\partial B$ near the phase transition. In other superconductors, the opposite happens, because the normal state magnetization is constant or decreases with T at constant applied field, whereas within the superconducting state, the magnetization grows with increasing T. The observed sign reversal in dB_{c2}/dT implies a significant additional field dependence of the entropy within the normal state. This might occur, for instance, if the system were tuned out of an additional ordered state, such as magnetic or quadrupolar order, by applied field, which would cause the entropy to increase over an intermediate field range.

HIGH PRESSURE HEAT CAPACITY MEASUREMENTS USING THE 3ω METHOD

Semi-quantitative measurements of the heat capacity under pressure in $CeSb_2$ were used to identify the observed kink in the temperature dependence of the resistivity as a thermodynamic phase transition and to track the pressure dependence of this phase transition. These measurements also showed evidence for a second phase transition at lower temperature, which has not been resolved in resistivity measurements and which disappears before the critical pressure associated with the upper phase transition is reached. Because the relaxation times of a small sample embedded in a pressure medium in a piston-cylinder pressure cell are too short to employ the standard pulse-relaxation method straightforwardly, the heat capacity was obtained using a temperature modulation technique.

A mg-sized single crystal of $CeSb_2$ was attached to a CX-1050 Lakeshore Cernox thermometer and a $200\,\Omega$ thin film heater with Devcon 5 Minute Epoxy. The three components were placed in the sample space of a piston cylinder cell with glycerol as a pressure medium. An AC current was supplied to the heater and the heat capacity of the sample was determined from the amplitude T_{AC} of the temperature oscillations in the thermometer and their phase α compared to the heater oscillations [4, 5] (Fig. 3).

The detection setup differed from the standard approach by using the same angular frequency ω to drive the heater current and to drive the thermometer measurement current. Because heater power oscillates at twice the heater current frequency ω, the temperature oscillations likewise occur at 2ω, causing resistance oscillations in the thermometer $R_{\mathrm{AC}}\cos(2\omega t - \alpha)$ on top of a DC resistance R_{DC}. The voltage drop across the thermometer therefore oscillates at the fundamental ω and at the third harmonic 3ω.

$$V = I_0\cos(\omega t)\left[R_{\mathrm{DC}} + R_{\mathrm{AC}}\cos(2\omega t - \alpha)\right] \tag{7}$$

$$= I_0\left[\left(R_{\mathrm{DC}} + \frac{R_{\mathrm{AC}}}{2}\right)\cos(\omega t) + \frac{R_{\mathrm{AC}}}{2}\cos(3\omega t - \alpha)\right]. \tag{8}$$

The third harmonic can be used to measure temperature oscillations in the thermometer. The method was originally employed in order to be able to do the measurements using a single lock-in amplifier with harmonic detection, but eventually, a second lock-in amplifier was used in order to make it easier to provide a separate supply of the heater current, which could then be controlled conveniently remotely. The preamplified signal monitor output from the first lock-in is fed into the input of Lock-in 2, which measures the r.m.s. amplitude of the third harmonic, $V_{3\omega}$. This can be used to calculate the amplitude of the resistance oscillations of the thermometer and thereby the size of the temperature oscillations:

$$V_{3\omega} = GI_0\frac{R_{AC}}{2\sqrt{2}} \quad , \tag{9}$$

where G is the preamplifier gain in Lock-in 1. The fundamental picked up by Lock-in 2 can be compared to the absolute amplitude detected by Lock-in 1 to determine the gain of the preamplifier.

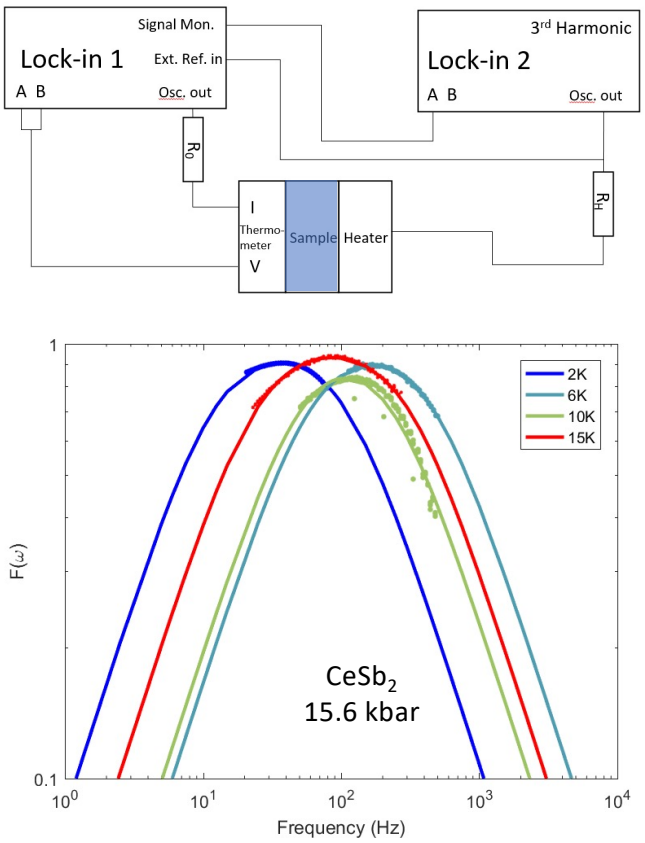

Figure 3. (Top) schematic of the signal detection setup for a temperature modulation heat capacity measurement using the 3ω method described in the text. Lock-in amplifier 1 is used to measure the resistance of a Cernox low temperature thermometer, which is driven at a frequency ω. Lock-in amplifier 2 drives a thick film heater at the same frequency ω. The two oscillators of lock-in amplifiers 1 and 2 are kept in synchrony by feeding the oscillator signal of lock-in 2 into the reference input of lock-in 1. The temperature signal is picked up by lock-in 1 but also passed (after pre-amplification) to lock-in 2, where the 3rd harmonic is detected. The 3rd harmonic provides an estimate of the heat capacity, as in the standard AC calorimetry method. (Bottom) typical frequency response observed in high pressure heat capacity measurements. The oscillation frequency ω should be chosen near the maximum in the response curve to minimise the consequences of drift, but the maximum is seen to shift slightly with temperature. The heater frequency was adapted accordingly during temperature sweeps. The peaked frequency response currently still limits the usefulness of the high pressure temperature modulation method for determining absolute values of the heat capacity, whereas phase transition anomalies can be resolved clearly.

Heater power is varied depending on temperature to keep the peak-to-peak temperature modulation amplitude within 2-3% of the current temperature. Typical heater power values were 5 µW at 0.5 K, 100 µW at 1 K and 500 µW at 5 K. As is described in some detail in [4], the frequency response of the temperature amplitude and phase can be thought of as resulting from a combination

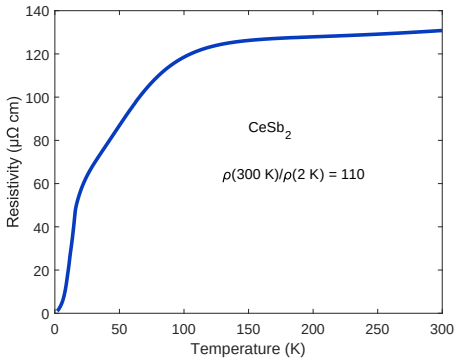

Figure 4. Resistivity versus temperature at ambient pressure recorded in a sample from a $CeSb_2$ growth batch used in high pressure measurements shown in the main paper.

of a high-pass filter caused by the short but finite relaxation time of sample against thermometer and heater, and a low-pass filter that results from the longer relaxation time of sample against environment. The frequency response was recorded at selected temperatures (Fig. 3) in order to be able to choose an excitation frequency near the maximum of the response, where drift in the conversion from temperature amplitude to heat capacity can be neglected to first order. Typical frequency choices for the heater current were ~ 10 Hz near the magnetic transition and ~ 100 Hz at higher temperatures. The superconducting transition itself could not yet be resolved, because the sensitive range of the thermometer is limited to temperatures $> T_c$.

$CeSb_2$ AMBIENT PRESSURE RESISTIVITY

Crystals of $CeSb_2$ were characterised at ambient pressure by in-plane resistivity measurements to extract the residual resistivity ratio (RRR). The resulting resistivity traces are consistent with traces reported in the literature (e.g. [6]) and show a distinct kink at the onset of magnetic order at $T \simeq 15.6$ K and further anomalies at lower temperature, associated with at least two more magnetic transitions (Fig. 4). RRR values scatter between between samples but we typically find RRR ~ 100 in the batches used to prepare the samples measured at high pressure.

[1] E. Helfand and N. R. Werthamer, Phys. Rev. **147**, 288 (1966).
[2] M. Tinkham, *Introduction to Superconductivity* (Dover Publications, 2004).
[3] T. P. Orlando, E. J. McNiff, S. Foner, and M. R. Beasley, Phys. Rev. B **19**, 4545 (1979).

[4] P. F. Sullivan and G. Seidel, Physical Review **173**, 679 (1968).
[5] E. Gati, G. Drachuck, L. Xiang, L.-L. Wang, S. L. Bud'ko, and P. C. Canfield, Review of Scientific Instruments **90**, 023911 (2019).
[6] S. L. Bud'ko, P. C. Canfield, C. H. Mielke, and A. H. Lacerda, Phys. Rev. B **57**, 13624 (1998).